Acta Cryst. (1982). A**38**, 337–345

Electric-Field-Induced Ionic Displacement and Redistribution of Bonding Electrons in $LiNbO_3$ and $LiTaO_3$ Revealed by Modulation X-ray Diffraction

BY ISAO FUJIMOTO

Broadcasting Science Research Laboratories of Nippon Hoso Kyokai, 1-10-11 *Kinuta, Setagaya-ku, Tokyo* 157, *Japan*

(*Received* 22 *August* 1981; *accepted* 2 *December* 1981)

Abstract

Electric fields with alternating square wave were applied to $LiNbO_3$ and $LiTaO_3$ single crystals in [001] directions, and extremely small ionic displacement was directly detected by the measurement of the diffracted intensities of X-rays synchronously with the applied fields. The displacement of Nb and Li ions relative to the oxygen framework were found to be $4{\cdot}9 \times 10^{-4}$ and 13×10^{-4} Å at $E = 51{\cdot}5$ kV cm^{-1} for $LiNbO_3$, and those of Ta and Li to be $6{\cdot}8 \times 10^{-4}$ and 15×10^{-4} Å at $E = 50$ kV cm^{-1} for $LiTaO_3$. The temperature factor was observed to vary with the external field, which is attributed to the change in phonon frequency of the crystal lattice. It was found from the intensity variations in the lower-indexed reflections that the displacements of the bonding electrons of Nb—O and Ta—O bonds are much larger than those of the constituent ions, which may be the origin of the electrooptic effect. The capability of the modulation technique in the absolute structure determination of crystals is demonstrated.

1. Introduction

Changes of crystal structures and electron redistribution induced by an externally applied field play a fundamental role in electronic and optical properties. Generally, such behaviour of electrons and atoms has only been inferred from the optical and electrical measurements, where indefiniteness remains. Therefore, the direct detection of the microscopic structural changes by X-ray diffraction has been desired. In fact there have been a few such measurements since the discovery of the diffraction of X-rays by crystals (Compton & Allison, 1935; Puget & Godefroy, 1975). However, no detail of the microscopic structural changes including the redistribution of valence electrons has been obtained, probably because the change in the diffracted intensities of X-rays caused by such structural changes are so small.

$LiNbO_3$ and $LiTaO_3$ are widely used as opto-electronic devices because of their large electrooptic effect, *i.e.* an electric-field-induced change in refractive index. Experimental and theoretical studies have shown that the effect is due to valence-electron redistribution associated with ionic displacement (DiDomenico & Wemple, 1972; Levine, 1973; 1974; Shih & Yariv, 1980). However, the most fundamental points of localized bond charge and its displacement are assumed *a posteriori* and do not rest on a foundation confirmed experimentally. The present author made an attempt to detect directly the electric-field-induced ionic displacement and electron redistribution in $LiNbO_3$ and $LiTaO_3$ by using a modulation method in the X-ray diffraction measurement and reported the preliminary results previously (Fujimoto, 1978). Here the full report of the study will be presented.

First the effect of the microscopic structural changes on the integrated intensities of X-rays are theoretically considered. Next, the experimental details are shown. It is desirable to have accurate structure data, without external fields, to obtain the microscopic structural changes. Therefore, the data determined by Abrahams *et al.* (Abrahams, Reddy & Bernstein, 1966; Abrahams & Bernstein, 1967; Abrahams, Hamilton & Sequeira, 1967) are refined by the measurement of the ratios of the diffracted intensities of X-rays from the two opposite surfaces, $(00h)$ and $(00\bar{h})$. Then the observed variations of the integrated intensities, $\Delta I/I$, are analysed first by assuming the ionic displacement alone and next by taking into account two other factors; one is the change in the temperature factor due to the electric-field-induced variation of phonon frequencies, and the other is the redistribution of bonding electrons of Nb—O and Ta—O bonds. Also, the effective charge is discussed in relation to polarization densities and the displacement of ions and bonding electrons. Furthermore, the modulation technique is demonstrated to be a new method of determining the absolute structure of crystals.

2. Theory

The structure factor of an hkl reflection can be given by

$$F_{\mathbf{h}} = \sum_j (f_j^0 + f_j' + if_j'') \, e^{-M_j} e^{2\pi i \mathbf{h}\cdot\mathbf{r}_j}, \quad (1)$$

$$M_j = B_j(\sin\theta/\lambda)^2, \quad (2)$$

0567-7394/82/030337-09$01.00

where $\mathbf{r}_j$ is the coordinate of the jth atom, f_j^0 is the atomic scattering factor, f_j' and f_j'' are the anomalous dispersion corrections and B_j is the temperature factor. When an external electric field is applied to the crystal, microscopic structural changes are induced, and we have the variation of the structure factor;

$$\Delta F_{\mathbf{h}} = \sum_j (f_j^0 + f_j' + if_j'')\, e^{-M_j} e^{2\pi i \mathbf{h}.\mathbf{r}_j}\, 2\pi i(\mathbf{h}.\Delta\mathbf{r}_j) + \sum_j \Delta(f_j^0 + f_j' + if_j'')\, e^{-M_j} e^{2\pi i \mathbf{h}.\mathbf{r}_j} - (\sin\theta/\lambda)^2 \times \sum_j (f_j^0 + f_j' + if_j'')\, e^{-M_j} e^{2\pi i \mathbf{h}.\mathbf{r}_j}\, \Delta B_j, \quad (3)$$

where the first term is due to the relative displacement of ions in the unit cell, the second one gives the change in the atomic scattering factor due to both the redistribution of electron densities (Buckingham, 1964) and the change of $\sin\theta/\lambda$ caused by piezoelectricity, and the third one gives the change in the temperature factor due to ionic displacement. By X-ray topography, the crystal used was found to be perfect enough for applying dynamical formulae (Cole & Stemple, 1962). This was confirmed by comparing intensities observed for $00h$ reflections with that for the 333 reflection of a perfect Si crystal. Therefore, the integrated reflecting power I for this experiment for $LiNbO_3$ and $LiTaO_3$ (symmetric Bragg case of non-centrosymmetric thick crystal) is given by

$$I = \frac{C\lambda^2(e^2/mc^2)|F_{\mathbf{h}}'|}{\pi V \sin 2\theta} R_{\mathbf{h}}, \quad (4)$$

where

$$R_{\mathbf{h}} = \frac{1 + k^2 + 2s}{[(1-k^2)^2 + 4p^2]^{1/2}} \int_{-\infty}^{\infty} \{L - (L^2 - 1)^{1/2}\}\, \mathrm{d}y, \quad (5)$$

$$L = \frac{[(y^2 - g^2 + k^2 - 1)^2 + 4(gy - p)^2]^{1/2} + (y^2 + g^2)}{[(1-k^2)^2 + 4p^2]^{1/2}}, \quad (6)$$

$$F_{\mathbf{h}} = F_{\mathbf{h}}' + iF_{\mathbf{h}}'', \quad (7)$$

$$F_{\mathbf{h}}' = \sum_j (f_j^0 + f_j')\, e^{-M_j} e^{2\pi i \mathbf{h}.\mathbf{r}_j} = |F_{\mathbf{h}}'|\, e^{i\alpha'}, \quad (8)$$

$$F_{\mathbf{h}}'' = \sum_j f_j''\, e^{-M_j} e^{2\pi i \mathbf{h}.\mathbf{r}_j} = |F_{\mathbf{h}}''|\, e^{i\alpha''}, \quad (9)$$

$$k = |F_{\mathbf{h}}''|/|F_{\mathbf{h}}'|, \quad (10)$$

$$s = -k \sin\delta, \quad (11)$$

$$p = k \cos\delta, \quad (12)$$

$$\delta = \alpha'' - \alpha', \quad (13)$$

$$g = \frac{-\mu V}{2(e^2/mc^2)\,\lambda |F_{\mathbf{h}}'|\, C}, \quad (14)$$

and the other symbols have their usual X-ray meaning. We can put $p \simeq |k|$ because δ is sufficiently small. Then we have

$$R_{\mathbf{h}}\,(\text{non-centrosymmetric}) \simeq \frac{1 + k^2 + 2s}{1 + k^2} R_{\mathbf{h}}\,(\text{centrosymmetric}), \quad (15)$$

where $R_{\mathbf{h}}$(centrosymmetric) is for $s = 0$ and $p = k$. Hereafter, $R_{\mathbf{h}}$ stands for $R_{\mathbf{h}}$(centrosymmetric). Then the variation of the integrated intensities associated with the microscopic structural changes can be expressed as

$$(\Delta I/I)_{\mathbf{h}} = -\frac{\Delta V}{V} - 2\cot 2\theta\, \Delta\theta + 2\frac{\Delta|F_{\mathbf{h}}|}{|F_{\mathbf{h}}|} - \frac{1-k^2}{1+k^2}\frac{\Delta|F_{\mathbf{h}}'|}{|F_{\mathbf{h}}'|} + \frac{C_\sigma \Delta R_{\mathbf{h}}^\sigma + C_\pi \Delta R_{\mathbf{h}}^\pi}{C_\sigma R_{\mathbf{h}}^\sigma + C_\pi R_{\mathbf{h}}^\pi} + \frac{\Delta C_\pi R_{\mathbf{h}}^\pi}{C_\sigma R_{\mathbf{h}}^\sigma + C_\pi R_{\mathbf{h}}^\pi}, \quad (16)$$

where

$$\Delta R_{\mathbf{h}} = \frac{\partial R_{\mathbf{h}}}{\partial k}\Delta k + \frac{\partial R_{\mathbf{h}}}{\partial |g|}\Delta|g| = -\left(\frac{\partial R_{\mathbf{h}}}{\partial k}k + \frac{\partial R_{\mathbf{h}}}{\partial |g|}|g|\right)\frac{\Delta|F_{\mathbf{h}}'|}{|F_{\mathbf{h}}'|} \equiv -D\frac{\Delta|F_{\mathbf{h}}'|}{|F_{\mathbf{h}}'|}, \quad (17)$$

by using the equation

$$|F_{\mathbf{h}}|^2 = |F_{\mathbf{h}}'|^2 (1 + k^2 + 2s), \quad (18)$$

and by assuming the variation of F_h'' to be negligibly small. The first, the second and the last terms are due to the variation of the lattice constant associated with piezoelectricity which can be evaluated easily, though they are small compared with the remaining terms. The remaining terms are due to the structural changes in the unit cell which can be deduced from (3). For example, for the change of the internal coordinates of the constituent atoms, $\Delta\mathbf{r}_j(\Delta x_{j1}, \Delta x_{j2}, \Delta x_{j3})$, the terms can be given explicitly as follows:

$$\frac{\Delta|F_{\mathbf{h}}|}{|F_{\mathbf{h}}|} = \sum_{k=1}^{3}\sum_j \frac{1}{|F_{\mathbf{h}}|}\frac{\partial|F_{\mathbf{h}}|}{\partial x_{jk}}\Delta x_{jk}$$
$$\frac{\Delta|F_{\mathbf{h}}'|}{|F_{\mathbf{h}}'|} = \sum_{k=1}^{3}\sum_j \frac{1}{|F_{\mathbf{h}}'|}\frac{\partial|F_{\mathbf{h}}'|}{\partial x_{jk}}\Delta x_{jk}, \quad (19)$$

and

$$\frac{\partial|F_{\mathbf{h}}|}{\partial x_{jk}} = \frac{1}{|F_{\mathbf{h}}|}\left(F_{\mathbf{h}r}\frac{\partial F_{\mathbf{h}r}}{\partial x_{jk}} + F_{\mathbf{h}i}\frac{\partial F_{\mathbf{h}i}}{\partial x_{jk}}\right)$$
$$\frac{\partial|F_{\mathbf{h}}'|}{\partial x_{jk}} = \frac{1}{|F_{\mathbf{h}}'|}\left(F_{\mathbf{h}r}'\frac{\partial F_{\mathbf{h}r}'}{\partial x_{jk}} + F_{\mathbf{h}i}'\frac{\partial F_{\mathbf{h}i}'}{\partial x_{jk}}\right), \quad (20)$$

where subscripts r and i denote the real and imaginary part, respectively. Then (16) becomes

$$(\Delta I/I)_{\mathbf{h}} - U_{\mathbf{h}} = \sum_{k=1}^{3} \sum_{j} A_{\mathbf{h}jk}\, \Delta x_{jk}, \tag{21}$$

where

$$U_{\mathbf{h}} = -\frac{\Delta V}{V} - 2 \cot 2\theta\, \Delta\theta + \frac{\Delta C_\pi R_{\mathbf{h}}^\pi}{C_\sigma R_{\mathbf{h}}^\sigma + C_\pi R_{\mathbf{h}}^\pi}, \tag{22}$$

and

$$A_{\mathbf{h}jk} = 2 \frac{1}{|F_{\mathbf{h}}|} \frac{\partial |F_{\mathbf{h}}|}{\partial x_{jk}} - \left(\frac{1-k^2}{1+k^2} + \frac{C_\sigma D^\sigma + C_\pi D^\pi}{C_\sigma R_{\mathbf{h}}^\sigma + C_\pi R_{\mathbf{h}}^\pi} \right) \times \frac{1}{|F'_{\mathbf{h}}|} \frac{\partial |F'_{\mathbf{h}}|}{\partial x_{jk}}. \tag{23}$$

From the measured values of $(\Delta I/I)_{\mathbf{h}}$ and the calculated values of $A_{\mathbf{h}jk}$, $\Delta \mathbf{r}_j$ can be obtained by the linear least-squares (LLSQ) analysis of (21).

3. Experimental

3.1. *Principle of the measurement*

The variations of the diffracted intensities of X-rays caused by the microscopic structural changes are too small to be detected by the conventional X-ray diffraction method. In order to overcome this difficulty, the present author developed a 'modulation method': Alternating electric fields in square waveform are applied to the specimen crystal, and the diffracted intensities in the two states for the top and the bottom of the square wave fields are measured by gating the two counters, A and B, synchronously with the external field. By taking the difference between the total counts of the counters, the small intensity variations can be measured (Figs. 1, 2). The long-term fluctuations in the incident X-ray beam intensity and electronic counting system can be eliminated. This method allows us to measure intensity variations as small as 0·01% by taking the measurement time sufficiently long.

3.2. *Experiment*

The experimental setup is shown schematically in Fig. 2. A high-power X-ray generator (Ag target, 60 kV, 500 mA maximum) was used. The specimen crystal was rotated around a Bragg position by an angle varying from 4 to 12′ to obtain the integrated intensities, and the modulated fractions were measured. The counting rates for the peak position ranged from 10^4 to 10^5 counts s^{-1} depending on the indices of reflections. To achieve a sufficient accuracy, the measurements were repeated automatically with use of a microcomputer.

Specimens were selected from various crystals by employing X-ray topography. The specimens are about 10 × 10 mm in size and 0·1–0·2 mm thick. The specimen surfaces, normal to the c axis, were polished and etched in a solution of $HF:2HNO_3$ at the boiling point. Aluminium was evaporated as electrodes on the two c faces, and the electric field was applied in the [001] direction normal to those faces.

3.3. *Piezoelectric constants and homogeneity of the fields*

In the measurement of the small intensity variation, we must avoid inhomogeneity of the field in the crystal caused by space charge which is often encountered with d.c. applied fields. Therefore, an alternating square-wave field was applied at a frequency of 19 Hz. To verify the homogeneity of the field, piezoelectric strains were determined by the measurement of the shift of the Bragg peak position, $\Delta\theta$, for $00h$ ($h = \pm 6, \pm 12, \ldots, \pm 42$) in reflection geometry and $h0\bar{h}0$ ($h = \pm 3, \pm 6, \pm 12$) in transmission geometry. In Fig. 3(a), the diffraction curves are shown corresponding to the two states of the opposite fields, A and B. Most of the

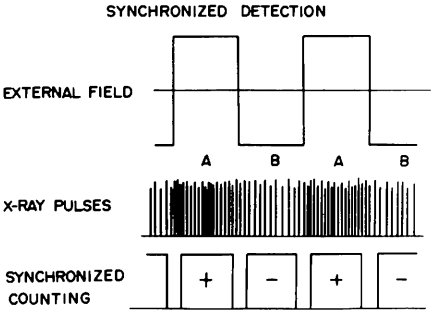

Fig. 1. Principle of synchronized detection.

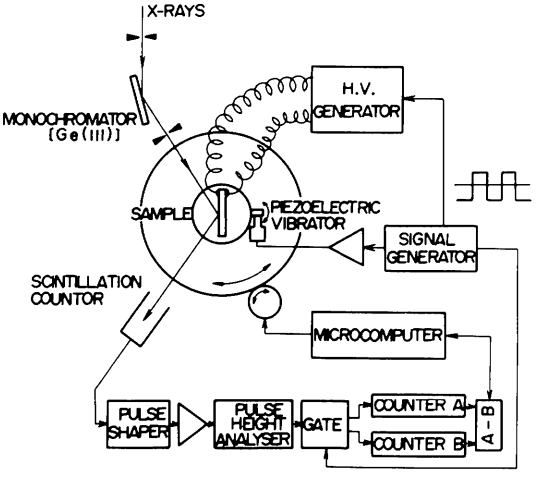

Fig. 2. Schematic view of the experimental setup.

difference in intensity between A and B at each angle, which is an apparently observed modulated intensity, arises from the shift of the reflection curve as shown in Fig. 3(b). The value of $\Delta\theta$ was easily obtained by comparing the intensity difference with the differential of the reflection curve without applied field, and found to satisfy the relationship

$$\Delta\theta = -\gamma \tan \theta_B, \tag{24}$$

as shown in Fig. 4. This corresponds to the differential of Bragg's law, $2d \sin \theta_B = \lambda$. From the variation of the lattice constants, $\Delta c/c$ and $\Delta a/a$, deduced from the relationship, the values of the piezoelectric constants d_{33} and d_{31} were found to be 8·4 pC N^{-1} and −0·77 pC N^{-1} for $LiNbO_3$, and 8·5 pC N^{-1} and −3·2 pC N^{-1} for $LiTaO_3$, respectively. These values are in reasonable agreement with those reported before by other authors (Warner, Onoe & Coquin, 1967; Yamada, Niizeki & Toyoda, 1967; Lissalde & Peuzin, 1976). It should be noted that the values of d_{33} obtained for the opposite faces agreed within an experimental uncertainty as shown in Fig. 4. These observations show that the electric field in the crystal was practically homogeneous.

Since the integrated intensities are affected little by the small shift of the Bragg angle if the integration range is sufficiently wide, the difference in the integrated intensities between the two states, A and B, is intrinsic to the microscopic structural changes. In practice the integration is made within a finite range of angle, and this gives a spurious result. To eliminate this effect, the specimen crystal was rotated by the angle $\Delta\theta$ [equation (24)] so as to position the Bragg peak at the centre of the integration range using a piezoelectric apparatus synchronized to the applied field; the B state was shifted to the B' position, as shown in Fig. 3, and the true modulated fraction, A–B', was measured.

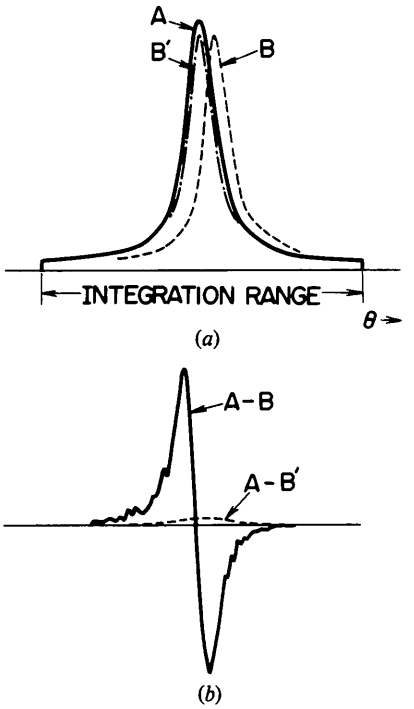

Fig. 3. (a) Reflection curves corresponding to the two states, A and B, with oppositely directed external fields. B' is the curve shifted from curve B by the piezoelectric apparatus. (b) Apparently observed modulated intensity (solid line) and the intrinsic one (dashed line).

4. Results

4.1. *Variation of the integrated intensities*

The modulated fractions of the integrated intensities are defined as

$$\Delta I/I = 2(I_+ - I_-)/(I_+ + I_-), \tag{25}$$

where I_+ and I_- represent the intensities with the external field parallel and antiparallel to the spontaneous polarization, respectively. They were measured for 00h reflections as shown in Fig. 5. The modulated fraction varies remarkably with reflection indices, reflecting the external-field-induced structural changes. To obtain the changes of the internal coordinates by the analysis of the results, accurate structure data without external field are necessary as described in § 2.

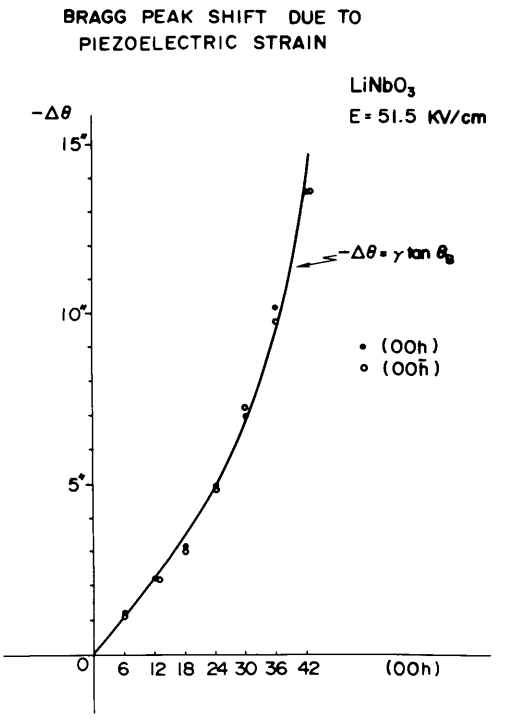

Fig. 4. Observed peak shifts of the Bragg diffraction curve due to piezoelectric strain vs reflection indices 00h for $LiNbO_3$. The solid line indicates the calculated vlaue with $\Delta d/d = 4{\cdot}32 \times 10^{-5}$.

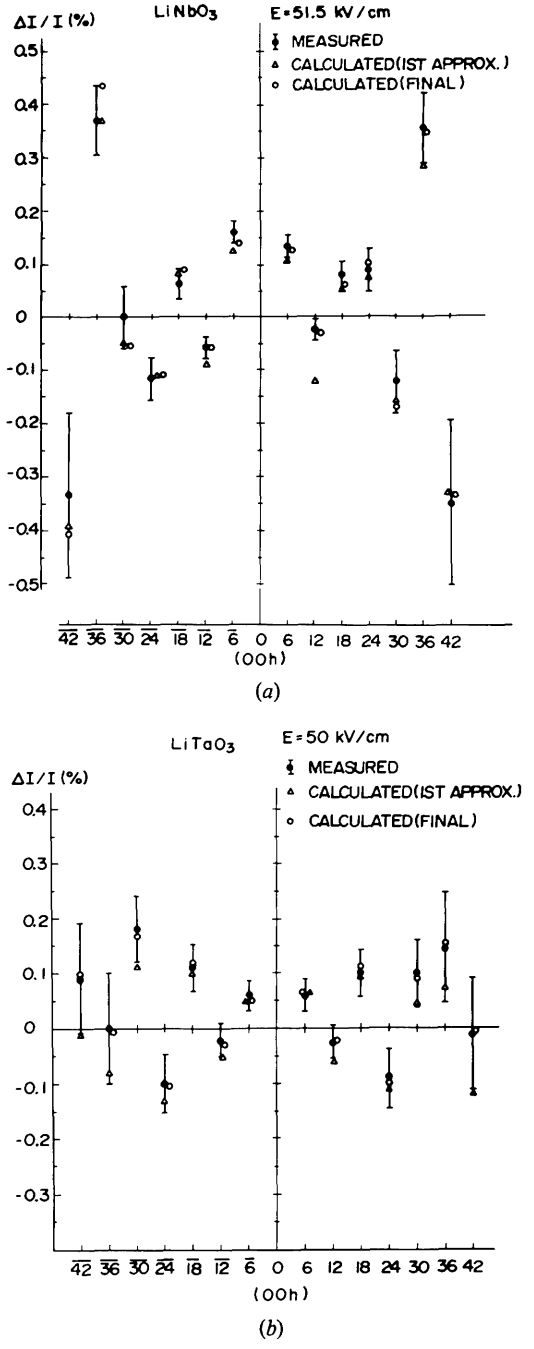

Fig. 5. Modulated fractions of the integrated intensities for $00h$ ($h = \pm 6, \pm 12, \ldots, \pm 42$) reflections for (*a*) $LiNbO_3$ and (*b*) $LiTaO_3$. Positive sign of $\Delta I/I$ shows the increase of the intensities when the direction of the applied field is parallel to the spontaneous polarization. △: The calculated value obtained by the linear-least-squares (LLSQ) analysis of the higher-indexed reflections ($\pm 00.18, \ldots, \pm 00.42$) with assumption of the displacement of rigid ions alone. Note the remarkable difference between the observed and calculated values for ± 00.12 reflections. ○: The calculated value obtained finally by the LLSQ analysis of all reflections taking into account not only the displacement of rigid ions but that of bonding electrons and the variation of the temperature factor.

Table 1. *Ratio of the integrated intensities of two opposite faces, $I(00h)/I(00\bar{h})$, for* $LiNbO_3$

$00h$	Abrahams *et al.*	Present work	Measured
$h = 6$	1·29	1·28	1·29 ± 0·01
12	0·86	0·86	0·85 ± 0·01
18	1·13	1·10	1·09 ± 0·01
24	0·80	0·93	0·93 ± 0·01
30	0·93	0·90	0·88 ± 0·01
36	1·92	1·41	1·40 ± 0·02
42	0·51	0·67	0·67 ± 0·02

4.2. *Crystal structure of* $LiNbO_3$ *and* $LiTaO_3$

According to Abrahams *et al.* (Abrahams, Reddy & Bernstein, 1966; Abrahams, Hamilton & Reddy, 1966; Abrahams & Bernstein, 1967; Abrahams, Hamilton & Sequeira, 1967), the crystals $LiNbO_3$ and $LiTaO_3$ have the symmetry of the noncentrosymmetric space group $R3c$ at room temperature: There are six molecules per hexagonal unit cell as illustrated in Fig. 6, where a unit of two molecules is shown.

In order to obtain accurate structure data along the c axis, the ratios of the integrated intensities for $00h$ and $00\bar{h}$ reflections were observed as shown in the last column of Table 1, because the ratios depend strongly on the positional coordinates. The ratio is related to the structure factors by the formula (Cole & Stemple, 1962)

$$I(00h)/I(00\bar{h}) = |F(00h)|^2/|F(00\bar{h})|^2. \quad (26)$$

Neglecting the small dispersion corrections for Li and O atoms, $F(00.\pm h)$ are given explicitly by

$$\begin{aligned} F(00.\pm h) = 6\{&3f^0(\mathrm{O})\exp[-B(\mathrm{O})(\sin\theta/\lambda)^2] \\ &+ f^0(\mathrm{Li})\exp[-B(\mathrm{Li})(\sin\theta/\lambda)^2] \\ &\times \exp[\pm 2\pi ihz(\mathrm{Li})] \\ &+ [f^0(\mathrm{Nb}) + f'(\mathrm{Nb})] \\ &\times \exp[-B(\mathrm{Nb})(\sin\theta/\lambda)^2] \\ &\times \exp[\pm 2\pi ihz(\mathrm{Nb})]\} \\ &+ 6if''(\mathrm{Nb})\exp[-B(\mathrm{Nb})(\sin\theta/\lambda)^2] \\ &\times \exp[\pm 2\pi ihz(\mathrm{Nb})]. \end{aligned} \quad (27)$$

It should be noted that $\sin\theta/\lambda$ dependence of $f''(\mathrm{Nb})$ was taken into account (Cooper, 1963, 1977).

Abrahams *et al.* (Abrahams, Reddy & Bernstein, 1966) gave the ionic coordinates along the c axis (taking one of the oxygen layers as $z = 0$) and the temperature parameters of $LiNbO_3$ as follows from X-ray diffraction studies:

$$\begin{aligned} &z(\mathrm{Nb}) = 0{\cdot}1019, \quad z(\mathrm{Li}) = 0{\cdot}3848, \\ &B(\mathrm{Nb}) = 0{\cdot}50\ \text{Å}^2, \quad B(\mathrm{O}) = 0{\cdot}43\ \text{Å}^2, \\ &B(\mathrm{Li}) = 0{\cdot}94\ \text{Å}^2. \end{aligned} \quad (28)$$

Using these values and taking f''(Nb) to be 2·86 (*International Tables for X-ray Crystallography*, 1974), we calculated the ratios $I_h/I_{\bar{h}}$ with (26) and compared them with the observed ratios in Table 1. Agreement between them was not sufficient. Therefore, the model of Abrahams *et al.*, together with f''(Nb), was corrected so as to fit the observed ratios by conventional least-squares analysis of (26), and the following results were obtained for $LiNbO_3$:

$$z(\mathrm{Nb}) = 0{\cdot}1035 \pm 0{\cdot}0003, \quad z(\mathrm{Li}) = 0{\cdot}3830 \pm 0{\cdot}0020,$$
$$B(\mathrm{Nb}) = 0{\cdot}35 \pm 0{\cdot}10\ \text{Å}^2, \quad B(\mathrm{O}) = 0{\cdot}57 \pm 0{\cdot}10\ \text{Å}^2$$
$$B(\mathrm{Li}) = 0{\cdot}70 \pm 0{\cdot}30\ \text{Å}^2, \quad f''(\mathrm{Nb}) = 2{\cdot}87 \pm 0{\cdot}05. \quad (29)$$

The good fit is seen from comparison between the third and fourth columns in Table 1. It should also be noted that the coordinates are close to those obtained by Abrahams *et al.* using neutron diffraction (Abrahams, Hamilton & Reedy, 1966).

For $LiTaO_3$, it is rather difficult to obtain accurate structure data from the observed ratios because the scattering factor of Ta is so large compared with those of Li and O that the ratios do not differ so much from unity as in the case of $LiNbO_3$. Therefore, only the z coordinates of Ta, on which the intensity ratios depend most, were refined by a similar analysis for the data obtained by Abrahams, Hamilton & Sequeira (1967). The results are as follows:

$$z(\mathrm{Ta}) = 0{\cdot}0971 \pm 0{\cdot}0003, \quad z(\mathrm{Li}) = 0{\cdot}3769,$$
$$B(\mathrm{Ta}) = 0{\cdot}32\ \text{Å}^2, \quad B(\mathrm{O}) = 0{\cdot}52\ \text{Å}^2,$$
$$B(\mathrm{Li}) = 1{\cdot}15\ \text{Å}^2, \quad f''(\mathrm{Ta}) = 4{\cdot}40. \quad (30)$$

5. Discussion

The structural change due to the applied electric fields is caused by both the displacement of the ions and that of the bonding electrons. First, the former will be analysed with the procedure described in § 2.

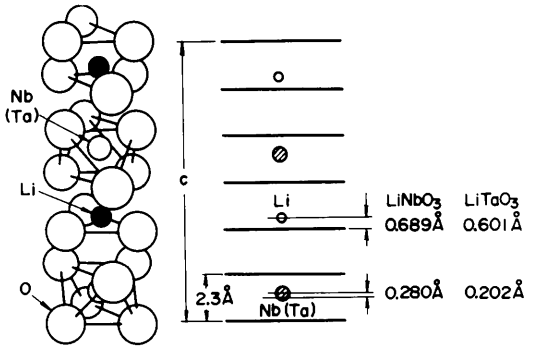

Fig. 6. Crystal structure of $LiNbO_3$ and $LiTaO_3$. A schematic view of a unit of two molecules along the c axis is shown.

5.1. *Ionic displacement and variation of the temperature factor*

In order to evaluate the ionic displacement by the electric fields, we assume, for the first approximation, that the change of the integrated intensities arises mainly from the displacement of rigid ions relative to each other. By denoting the displacements of Nb, Ta and Li ions along the z direction relative to the oxygen framework by Δz(Nb), Δz(Ta) and Δz(Li), the derivatives $\partial F_{hr}/\partial x_{jk}$, $\partial F_{hi}/\partial x_{jk}$, $\partial F'_{hr}/\partial x_{jk}$ and $\partial F'_{hi}/\partial x_{jk}$ for $\pm 00h$ reflections in (19)–(23) are given explicitly as follows, from (27):

$$\frac{\partial F_{hr}}{\partial z(\mathrm{Nb})} = -12\pi h \exp[-B(\mathrm{Nb})(\sin\theta/\lambda)^2] \times \{[f^0(\mathrm{Nb}) + f'(\mathrm{Nb})]\sin 2\pi h z(\mathrm{Nb}) \pm f''(\mathrm{Nb})\cos 2\pi h z(\mathrm{Nb})\}$$

$$\frac{\partial F_{hi}}{\partial z(\mathrm{Nb})} = 12\pi h \exp[-B(\mathrm{Nb})(\sin\theta/\lambda)^2] \times \{\pm[f^0(\mathrm{Nb}) + f'(\mathrm{Nb})]\cos 2\pi h z(\mathrm{Nb}) - f''(\mathrm{Nb})\sin 2\pi h z(\mathrm{Nb})\}$$

$$\frac{\partial F_{hr}}{\partial z(\mathrm{Li})} = -12\pi h \exp[-B(\mathrm{Li})(\sin\theta/\lambda)^2] \times f^0(\mathrm{Li})\sin 2\pi h z(\mathrm{Li})$$

$$\frac{\partial F_{hi}}{\partial z(\mathrm{Li})} = \pm 12\pi h \exp[-B(\mathrm{Li})(\sin\theta/\lambda)^2] \times f^0(\mathrm{Li})\cos 2\pi h z(\mathrm{Li})$$

$$\frac{\partial F'_{hr}}{\partial z(\mathrm{Nb})} = -12\pi h \exp[-B(\mathrm{Nb})(\sin\theta/\lambda)^2] \times [f^0(\mathrm{Nb}) + f'(\mathrm{Nb})]\sin 2\pi h z(\mathrm{Nb})$$

$$\frac{\partial F'_{hi}}{\partial z(\mathrm{Nb})} = \pm 12\pi h \exp[-B(\mathrm{Nb})(\sin\theta/\lambda)^2] \times [f^0(\mathrm{Nb}) + f'(\mathrm{Nb})]\cos 2\pi h z(\mathrm{Nb})$$

$$\frac{\partial F'_{hr}}{\partial z(\mathrm{Li})} = \frac{\partial F_{hr}}{\partial z(\mathrm{Li})}, \quad \frac{\partial F'_{hi}}{\partial z(\mathrm{Li})} = \frac{\partial F_{hi}}{\partial z(\mathrm{Li})}. \quad (31)$$

For $LiTaO_3$, the index of Nb should be replaced by Ta.

Now we can evaluate A_{hjk} in (21) from (29), (30) and (31). Using the observed values for $(\Delta I/I)_h$ on the left hand side of (21), we calculated the displacement of ions by the linear-least-squares fitting method by taking the weighting factor as the inverse of the standard deviation. Fairly large discrepancies between the observed and calculated values of the intensity change were found for lower-indexed reflections, which is due to the effect of the redistribution of the outer electrons.

To obtain the displacement of rigid ions, therefore, LLSQ analysis was made, for the second step, only for the higher-order indexed reflections (±00.18, ..., ±00.42), which arise predominantly from the inner, more tightly bound electrons (ion core). The results are shown in Table 2 and denoted by the triangles in Fig. 5.*

We now consider the differences between the observed and calculated values in Fig. 5. The remarkable difference for 00.12 reflections for both $LiNbO_3$ and $LiTaO_3$ is due to redistribution of outer electrons as will be discussed later. Furthermore, a systematic difference is seen for the higher-order reflections, especially for $LiTaO_3$: the observed values are larger than the calculated values, and the difference becomes larger as the reflection indices become higher. This tendency can be explained by assuming that the temperature factor is changed by the external field; since the positions of cations are deviated from symmetry in the positive z direction, their further displacement in that direction by the external field make the crystal lattice more 'rigid' than that in the opposite direction. Then, the lattice vibration has higher frequencies and smaller amplitudes, and the diffracted intensities of X-rays increase. Therefore, by taking into account the variation of the temperature factor, ΔB(Nb) and ΔB(Ta), in the LLSQ analysis, we have better agreement of the calculated and observed values of $\Delta I/I$ for higher-order reflections; the best fit was obtained for $\Delta B(\mathrm{Nb}) = -0{\cdot}6 \times 10^{-4}$ Å^2 and $\Delta B(\mathrm{Ta}) = -3 \times 10^{-4}$ Å^2. Since the temperature factor B is nearly proportional to $\sum_j (kT/\omega_j^2)$, where ω_j is the phonon frequency of the jth mode, the shift of the phonon frequency of the order of 10^{-3} at $E = 50$ kV cm^{-1} may be expected from the calculated value of ΔB. Such a frequency shift is supported from the experimental result by Raman scattering that the phonon frequencies of ferroelectric modes in some perovskite-type crystals depend markedly on applied electric fields (Worlock & Fleury, 1967). It should be noted that the tendency mentioned above is more evident in $LiTaO_3$ than in $LiNbO_3$. Although these substances have isomorphic crystal structures and many similarities, they also show significant differences in thermal and optical properties, which may be correlated with the differences in thermal vibration observed here.

* It is noteworthy that a thermal diffuse scattering (TDS) correction for the integrated intensities was not made. This results in an error of only 3% in the ionic displacement for Nb and Ta, and 5% for Li ions.

Table 2. *Calculated values of the change of the internal parameters and the reliability factor* $R = \sum_h |(\Delta I/I)_o - (\Delta I/I)_c| / \sum_h |(\Delta I/I)_o|$ *for* $LiNbO_3$ ($E = 51{\cdot}5$ kV cm^{-1}) *and* $LiTaO_3$ ($E = 50$ kV cm^{-1})

(1) Values obtained by LLSQ analysis of the higher-indexed reflections (±00.18, ..., ±00.42) with assumption of the displacement of rigid ions alone.
(2) Values obtained by LLSQ analysis of all reflections by taking into account not only the displacement of rigid ions but that of bonding electrons and the variation of the temperature factor.

	$LiNbO_3$		$LiTaO_3$	
	(1)	(2)	(1)	(2)
Δz(Nb)				
Δz(Ta)	4·5 ± 0·4	4·9 ± 0·4	6·6 ± 0·5	6·8 ± 0·5
Δz(Li)	9·2 ± 2·0	13 ± 2·0	16 ± 5·0	15 ± 5·0
Δz(bond)		−230		−230
ΔB(Nb)		−0·58		−2·9
ΔB(Ta)				
R	0·21	0·17	0·58	0·08

Δz in units of 10^{-4} Å; ΔB in units of 10^{-4} Å^2.

5.2. *Effective charge and redistribution of bonding electrons*

From the results obtained above on the assumption of the displacement of rigid ions, the effective charge of the constituent cations are evaluated on the basis of a simple theory of dielectrics; the ionic polarization density P_i is given by

$$P_i = (6/V) \sum_j Q(M_j)\, \Delta z(M_j), \tag{32}$$

where $Q(M_j)$ is the charge, $\Delta z(M_j)$ is the magnitude of displacement of Nb, Ta and Li ions, and V is the volume of the hexagonal unit cell. On the other hand, P_i can be deduced from the difference between the static and optical dielectric constants, $\kappa_0 - \kappa_\infty$, as

$$P_i = \varepsilon_0(\kappa_0 - \kappa_\infty)\, E. \tag{33}$$

Using the value of κ_0 and κ_∞ (Landolt-Börnstein, 1969), we calculated P_i to be 1·15 mC m^{-2} at $E = 51{\cdot}5$ kV cm^{-1} for $LiNbO_3$, and 1·80 mC m^{-2} at $E = 50$ kV cm^{-1} for $LiTaO_3$.

Substituting P_i and the values of Δz obtained above into (32), Q(Nb) and Q(Ta) were evaluated to be 6·4 and 6·6, rspectively, by putting Q(Li) = 1·0 because the Li–O bond can be considered to be purely ionic. It should be noted that the smaller effect of atomic polarization due to the displacement of the centre of the core electrons from the position of the nucleus (Buckingham, 1964) was neglected. Kahn & Leyendecker (1964) showed in the electronic energy-band calculation of $SrTiO_3$, which has a typical structure homologous to $LiNbO_3$, that substantial covalency between O anions and Ti cations was to be expected. Peterson *et al.* (Peterson, Bridenbaugh & Green, 1967; Peterson & Bridenbaugh, 1968) obtained the net charge of Nb and Ta to be 1·6 and 1·2, respectively, by the study of ^{7}Li nuclear magnetic resonance in $LiNbO_3$ and

$LiTaO_3$, and concluded that Nb and Ta ions were predominantly covalently bonded. The difference between the charge of cations obtained by Peterson *et al.* and those evaluated above is expected to arise from the neglect of the deformation of valence electrons associated with ionic displacement in the evaluation of polarization densities.

This behaviour of valence electrons has been predicted to play an important role in the dielectric and optical properties of various compounds on the basis of the bond charge theory developed by Phillips (Phillips, 1968, 1973; Levine, 1973, 1974; Shih & Yariv, 1980). The difference between the observed and calculated values of the change of X-ray intensities for ± 00.12 reflections described above can be considered to show the direct evidence of this redistribution of valence electrons because those reflections are sensitive to valence electron distribution as shown in the following.

We estimate roughly the redistribution of bonding electrons. First, we assume the localized bond charge at the midpoint of Nb—O and Ta—O bonds. The structure factors are given by

$$F(00h) = 6\{F(\text{ion}) + 3(f_{b_1} + f_{b_2}) \exp(2\pi i h z_{b_1})\}, \quad (h = \pm 12), \tag{34}$$

where b_1 and b_2 denote the bonds with long and short bond length, respectively. Since we have no data about the bond charge of Nb—O and Ta—O bonds, we take them, for the first approximation, to be that of Si, which was given by Hattori, Kuriyama, Katagawa & Kato (1965) as

$$f_b = 0{\cdot}45 \exp[-13(\sin\theta/\lambda)^2] \tag{35}$$

though indefiniteness still remains.* Furthermore, for simplicity, the scattering amplitude and the magnitude of displacement were assumed to be the same for two kinds of bond position. Schematic representation of the structure factor of ± 00.12 reflections including bonding electrons are shown in Fig. 7. It can readily be seen that the effect of the displacement of bonding electrons on the 00.12 reflection is much larger than that on $00.\bar{1}\bar{2}$, in agreement with the present measurement. Thus, least-squares analysis was made finally for the observed change of the integrated intensities by taking into account an additional parameter of the displacement of the bonding electrons, Δz(bond). The result is shown in Table 2 and denoted in Fig. 5 by circles; the calculated values of $\Delta I/I$ for ± 00.12 reflections are in good agreement with the observed one, and Δz(bond) obtained is much larger than Δz(ion). It should be noted that the analysis has only qualitative meaning because the calculated value of Δz(bond) depends on the bond position and f_b. However, it is noteworthy that even a much larger value of Δz(bond) will be obtained considering that the bond charge of Nb—O and Ta—O bonds are expected to be smaller than that of purely covalent crystal of Si. This large displacement of bonding electrons can be thought to be the origin of the microscopic mechanism responsible for the electro-optic effect, *i.e.* the change of the refractive index due to the external field (DiDomenico & Wemple, 1972).

5.3. *Differential structure analysis*

It seems worth discussing the capabilities of the present method for the precise determination of crystal structures. The microscopic structural changes obtained by the analysis of the changes in the diffracted intensities of X-rays depend largely on the original coordinates of the atoms without applied fields, as described before. As an example, the observed values of $\Delta I/I$ for $LiNbO_3$ were analysed on the basis of the structural data given by Abrahams *et al.* for comparison with the results obtained above. The results are as follows: $\Delta z(\text{Nb}) = 3{\cdot}1 \times 10^{-4}$ Å, $\Delta z(\text{Li}) = 30 \times 10^{-4}$ Å, $\Delta z(\text{bond}) = -200 \times 10^{-4}$ Å and $\Delta B = 0{\cdot}43 \times 10^{-4}$ Å^2. The agreement between the observed and the calculated intensity change was found to be poorer than those based on the present model; the agreement factor, $R = \sum_h |(\Delta I/I)_o - (\Delta I/I)_c| / \sum_h |(\Delta I/I)_o|$, was evaluated to be 0·24 compared with 0·17 for the present model. Moreover, the difference between the calculated and the observed change is comparatively large for the 00.42 reflection; the calculated value of $\Delta I/I$ is $-0{\cdot}63$ whereas the observed one is $-0{\cdot}35$. These indicate that the present model is closer to the real structure than those of Abrahams *et al.* Thus, the change in the diffracted intensities of X-rays associated with the displacement of the constituent atoms reflects sensitively the original coordinates of the constituent atoms.

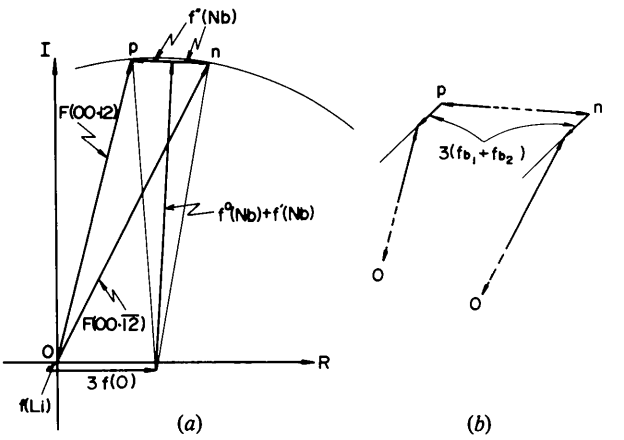

Fig. 7. (*a*) Schematic representation of the structure factor of ± 00.12 reflections for $LiNbO_3$. $F(00.\bar{1}\bar{2})$ is shown with the imaginary axis inverted. (*b*) Enlarged (×10) diagram around *p* and *n* points in (*a*) to show the effect of the bonding electrons.

* The precise measurement of the structure factor of Si 222 forbidden reflection by the *Pendellösung*-fringe method gives a 20% smaller value (Fujimoto, 1974).

The characteristics of the present method described above can also be used for the determination of absolute structure. This is shown schematically in Fig. 8 as a demonstration of the simple case of the binary compound AB, where F_A and F_B represent the structure factors of A and B atoms, respectively, and φ_B the phase angle of B atoms relative to A. If we have two possible cases of atomic configurations corresponding to the two phase angles, φ_{B_1} and φ_{B_2}, the structure factors, F_1 and F_2, have the same absolute value so that identification of them is difficult by the conventional integrated intensity measurements. However, when B atoms are displaced in the direction of, say, increasing the phase angle by the external force, the structure factor decreases in case 1, and increases in case 2, so that we can determine very easily which one is the real structure by observing the intensity change. Thus, the present modulation technique could be used as a new method in determining the absolute configuration of the crystal structure.

6. Conclusion

The modulation X-ray diffraction method was proved to be useful in the study of the dynamical properties of a crystal; electric-field-induced microscopic structural changes such as extremely small ionic displacement ($\sim 10^{-4}$ Å) and variation of the temperature factor were directly detected for the displacive ferroelectrics of $LiNbO_3$ and $LiTaO_3$. Large displacement of bonding electrons of Nb–O and Ta–O bonds associated with the displacement of the constituent ions was found, which is thought to be the origin of the microscopic mechanism responsible for the electrooptic effect.

Since the variation of the diffracted intensities associated with the displacement of the constituent atoms induced by the external field reflects sensitively the original coordinates of the crystal structure, the present modulation technique will be used not only as a useful technique in the study of the dynamical behaviour of crystals but also as a new method in determining the absolute configuration of the crystal structure.

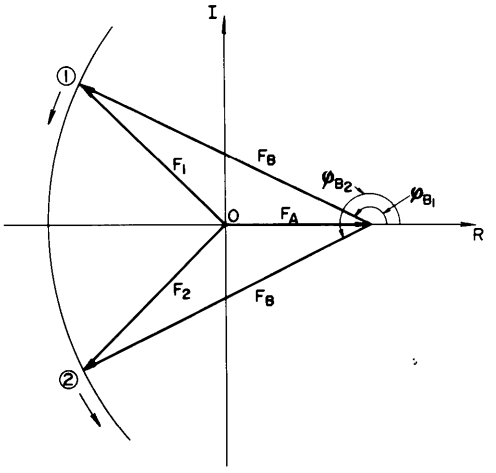

Fig. 8. Principle of the differential structure analysis.

The author wishes to thank Dr J. Chikawa for the critical reading of this manuscript and Dr S. Tatsuoka for his encouragement through this work.

References

ABRAHAMS, S. C. & BERNSTEIN, J. L. (1967). *J. Phys. Chem. Solids*, **28**, 1685–1692.

ABRAHAMS, S. C., HAMILTON, W. C. & REDDY, J. M. (1966). *J. Phys. Chem. Solids*, **27**, 1013–1018.

ABRAHAMS, S. C., HAMILTON, W. C. & SEQUEIRA, A. (1967). *J. Phys. Chem. Solids*, **28**, 1693–1698.

ABRAHAMS, S. C., REDDY, J. M. & BERNSTEIN, J. L. (1966). *J. Phys. Chem. Solids*, **27**, 997–1012.

BUCKINGHAM, A. D. (1964). *Acta Cryst.* **17**, 960–962.

COLE, H. & STEMPLE, N. R. (1962). *J. Appl. Phys.* **33**, 2227–2233.

COMPTON, A. H. & ALLISON, S. K. (1935). *X-rays in Theory and Experiment*, 2nd ed., pp. 469–471. New York: Van Nostrand.

COOPER, M. J. (1963). *Acta Cryst.* **16**, 1067–1069.

COOPER, M. J. (1977). *Acta Cryst.* A**33**, 229–230.

DIDOMENICO, M. JR & WEMPLE, S. H. (1972). *Applied Solid State Science* 3, edited by R. WOLFE, pp. 263–383. New York: Academic Press.

FUJIMOTO, I. (1974). *Phys. Rev. B*, **9**, 591–599.

FUJIMOTO, I. (1978). *Phys. Rev. Lett.* **40**, 941–944.

HATTORI, H., KURIYAMA, H., KATAGAWA, T. & KATO, N. (1965). *J. Phys. Soc. Jpn*, **20**, 988–996.

International Tables for X-ray Crystallography (1974). Vol. IV. Birmingham: Kynoch Press.

KAHN, A. H. & LEYENDECKER, A. J. (1964). *Phys. Rev.* **135**, A1321–A1325.

LANDOLT-BÖRNSTEIN (1969). *Numerical Data and Functional Relationships in Science and Technology*, Group III, Vol. 3, edited by K.-H. HELLWEGE & A. H. HELLWEGE. Heidelberg: Springer.

LEVINE, B. F. (1973). *Phys. Rev. B*, **7**, 2600–2626.

LEVINE, B. F. (1974). *Phys. Rev. B*, **10**, 1655–1664.

LISSALDE, F. & PEUZIN, J. C. (1976). *Ferroelectrics*, **14**, 579–582.

PETERSON, G. E. & BRIDENBAUGH, P. M. (1968). *J. Chem. Phys.* **48**, 3402–3406.

PETERSON, G. E., BRIDENBAUGH, P. M. & GREEN, P. (1967). *J. Chem. Phys.* **46**, 4009–4014.

PHILLIPS, J. C. (1968). *Phys. Rev.* **166**, 832–838.

PHILLIPS, J. C. (1973). *Bonds and Bands in Semiconductors*. New York: Academic Press.

PUGET, R. & GODEFROY, L. (1975). *J. Appl. Cryst.* **8**, 297–303.

SHIH, C.-C. & YARIV, A. (1980). *Phys. Rev. Lett.* **44**, 281–284.

WARNER, A. W., ONOE, M. & COQUIN, G. A. (1967). *J. Acoust. Soc. Am.* **42**, 1223–1231.

WORLOCK, J. M. & FLEURY, P. A. (1967). *Phys. Rev. Lett.* **13**, 1176–1179.

YAMADA, T., NIIZEKI, N. & TOYODA, H. (1967). *Jpn. J. Appl. Phys.* **6**, 151–155.